Review of magnetostrictive materials for structural vibration control

Topical Review

Review of magnetostrictive materials for structural vibration control

Zhangxian Deng and Marcelo J Dapino

NSF IUCRC Smart Vehicle Concepts Center, Department of Mechanical and Aerospace Engineering, The Ohio State University, Columbus, OH 43210, United State of America

E-mail: dapino.1@osu.edu

Abstract

Excessive vibrations in civil and mechanical systems can cause structural damage or detrimental noise. Structural vibrations can be mitigated either by attenuating energy from vibration sources or isolating external disturbance from target structures. Magnetostrictive materials coupling mechanical and magnetic energies have provided innovative solutions to vibration control challenges. Depending on the system's tunability and power consumption, the existing vibration control strategies are categorized into active, passive, and semi-active types. This article first summarizes the unique properties of magnetostrictive materials that lead to compact and reliable vibration control strategies. Several magnetostrictive vibration control mechanisms together with their performance are then studied using lumped parameter models. Finally, this article reviews the current state of vibration control applications utilizing magnetostrictive materials, especially Terfenol-D and Galfenol.

(Some figures may appear in colour only in the online journal)

1. Introduction

Low-frequency seismic impacts can cause devastating structure damage in buildings. Structural vibrations in mechatronic systems, on the other hand, exhibit a broader frequency range and may cause excessive detrimental noise. For certain applications, such as surgical equipment and atomic force microscopy, structural vibrations can lead to undesirable fluctuation and degrade motion control accuracy. The aforementioned negative effects can be mitigated by various vibration control mechanisms.

The vibration control systems can be categorized as vibration compensation, frequency tuning, structural damping, vibration isolation, and vibration absorption [1]. A vibration compensation system (e.g., vibration compensation lens) directly generates a force or varying stiffness that counteracts the external disturbance. Frequency tuning method controls the system natural frequencies and avoids resonance due to external excitations. The frequency can be tuned either by changing the mass m or stiffness k. The frequency tuning usually targets a specific system resonance; introducing structural damping c to the system (e.g., hydraulic dashpots) can convert vibration energy to heat and thus reduce the vibration amplitude over a broad frequency range. Vibration isolation either separates vibration sources from primary structures (e.g., car engine mounts) or protects the primary structure from base excitation (e.g., car suspension). Vibration absorbers, on the other hand, suppress structural vibration by attaching a damped vibration neutralizer or damped dynamic vibration absorber, which is simply an additional spring-damper-mass system.

Smart materials coupling mechanical energy with other energy forms have been investigated in vibration control. Depending on system tunability and power consumption, the existing smart vibration control systems can be categorized into three different types: active, passive, and semi-active. Active isolators or absorbers, as shown in figure 1, generate a force $F(t)$ that counteracts the disturbances [2, 3]. Unlike

1
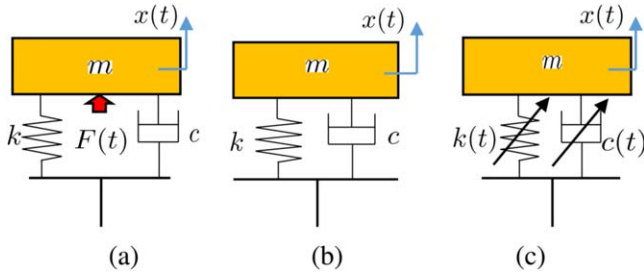
Figure 1. Lumped parameter model of (a) active, (b) passive, and (c) semi-active vibration control strategies. $F(t)$ is the actuation force, $k(t)$ is a tunable spring, and $c(t)$ is a tunable damper.

conventional passive servo-hydraulic actuators or electrical motors, smart materials enable vibration control strategies with small packaging size, broad frequency bandwidth, and high reliability. Shape memory alloys, which typically exhibit large deformation (up to 6%) but low operation frequencies, have been implemented to reduce seismic vibrations in buildings [4]. Piezoelectric materials, which provide large forces and moderate displacements at extremely high frequencies, have been utilized to design lightweight and dynamic actuators for mechatronic systems [5, 6] or civil applications [7]. But piezoelectric materials suffer from depolarization and brittleness thus exhibiting limited reliability.

Smart active vibration control requires external power sources and sometimes complex controllers which are not always available in practice. Thus, smart passive vibration control shown in figure 1(b), which is more convenient has been studied. Conventional passive vibration control can be achieved by adding damping materials, such as fluids and viscoelastic materials, to the primary structure. These passive materials provide a large damping coefficient c while exhibiting low stiffness and introducing redundant mass. Smart materials have been implemented as passive damping materials either through energy coupling or superelasticity. Piezoelectric materials [8] and piezoelectric polymers [9] attenuate vibration energy via intrinsic hysteresis and electro-mechanical energy coupling in shunt circuits. However, the piezoelectric materials are not suitable for complex loadings due to their brittleness. Shape memory alloys, which exhibit superelasticity during phase transition, are able to provide large damping but extremely low stiffness [10].

Smart active vibration control requires large control efforts and may cause control-induced instability. Smart passive vibration control, on the other hand, is not adaptive to the variation of system parameters and uncertainties in vibration sources. Semi-active vibration control lifts these limitations by creating tunable springs or dampers, as shown in figure 1(c). Since the semi-active mechanisms do not directly act against the vibration sources, little or no external power is required [11]. Smart materials integrated with passive mechanisms have been implemented in semi-active vibration control. Giurgiutiu *et al* [12] connected shape memory alloys with morphing mechanisms to mitigate structural vibrations in helicopter blades. However, shape memory alloys exhibit a low operating frequency and need a

mechanism to provide restoring forces. Recent studies have presented other possible semi-active vibration control methods by directly tuning the material properties of smart materials. Magnetorhelogical (MR) materials, which are iron particles embedded elastomers or fluids, are able to provide magnetically-tunable stiffness and damping coefficient [13, 14]. Asnani *et al* [15] showed that the stiffness and damping coefficient of piezoelectric materials can be continuously tuned by adjusting electrical shunts.

Table 1 summarizes the merits and drawbacks of selected smart materials in three different types of vibration control strategies. Magnetostrictive materials coupling mechanical and magnetic energies are able to tackle the drawbacks associated with the existing smart solutions. This article reviews the state of the art of magnetostrictive materials, especially Terfenol-D and Galfenol, in structural vibration control. The unique material properties of magnetostrictive materials and the resulting vibration control strategies are discussed in section 2. The vibration control systems are investigated following lumped parameter modeling in section 3. Configurations of magnetostrictive devices for vibration control are summarized and compared in section 4.

## 2. Properties of magnetostrictive materials

Magnetostrictive materials can be approximated by a collection of magnetic domains whose orientations depend on the interplay of magnetic and mechanical energies. The magneto-mechanical coupling induces several unique behaviors that are relevant to structural vibration control: the Joule effect, the Villari effect, material hysteresis, and the Delta-E effect.

2.1. Joule magnetostriction

As the applied magnetic field increases, magnetic domains tend to rotate toward the field direction, resulting in a dimensional change. The field-induced strain, or magnetostriction, includes the longitudinal component $\lambda_\parallel$ and the transverse component $\lambda_\perp$. To maintain volume consistency, $\lambda_\perp = -0.5\lambda_\parallel$. All magnetic materials demonstrate magneto-mechanical coupling, but a few materials containing rare earth elements show significant magnetostriction. Terbium, iron, and dysprosium alloys, or Terfenol-D, are able to generate a maximum magnetostriction of 1600×10^{-6} while requiring a high excitation magnetic field ($\approx 160 \, \mathrm{kA/m}$) [16]. Terfenol-D is brittle and can only withstand compressive axial loads. Iron-gallium alloys, known as Galfenol, exhibit moderate magnetostriction and mechanical robustness [17]. The magnetostriction of Galfenol varies with respect to gallium content, peaking around 18.6% gallium [18]. A maximum magnetostriction of 350×10^{-6} and 400×10^{-6} can be achieved from polycrystalline and single crystal Galfenol, respectively. Galfenol has high tensile strength of about 500 MPa and thus is able to support shear and tensile loads. Similar to steel, Galfenol can be machined, welded, and formed without the loss of magnetostriction. Figure 2 shows the field-induced magnetostriction of a polycrystalline
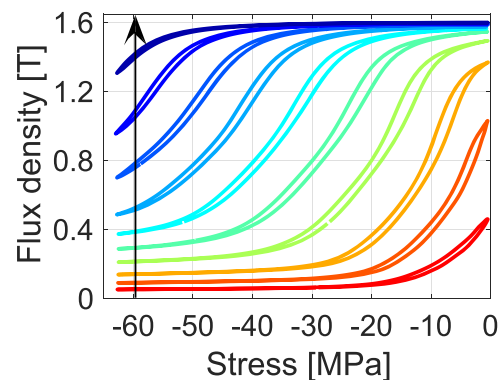
Table 1. Comparison of smart materials in vibration control. (*Only applies to certain magnetostrictive materials, such as Galfenol and Alfenol).

	Active	Passive	Semi-active
Shape memory alloy	Thermally-activated Large strain Low frequency	Superelasticity Large damping Low stiffness	With tuning mechanism Large packaging size
MR elastomer	N/A		Magnetically-tunable Wireless and non-contact Low stiffness
Piezoelectric	Voltage activated High frequency and stiffness	Hysteresis and energy coupling Moderate strain	Electrically-tunable Brittleness and low reliability
Magnetostrictive	Magnetically-activated High stiffness and moderate strain	Hysteresis, eddy currents, and energy coupling Machinable and non-contact	Magnetically-, mechanically-, or electrically-tunable Mechanically-robust and reliable
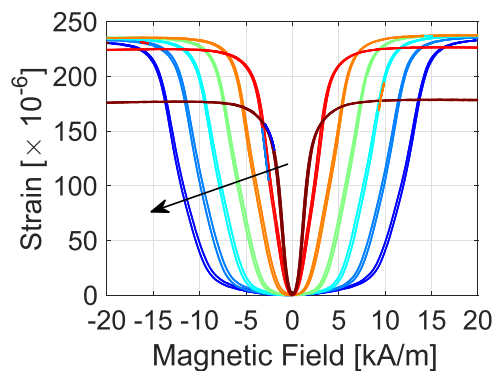
Figure 2. Magnetostriction versus magnetic field curves of a $\langle 100 \rangle$-oriented and polycrystalline $Fe_{81.4}Ga_{18.6}$ Galfenol rod [19]. The applied bias stresses are -1.64, -10.23, -20.44, -30.65, -40.88, -51.10, and -61.31 MPa. The arrow indicates the increasing bias mechanical stress.

Figure 3. Flux density versus stress curves of $\langle 100 \rangle$-oriented and polycrystalline $Fe_{81.4}Ga_{18.6}$ Galfenol rod [19]. The bias magnetic fields are 0.73, 1.42, 2.41, 3.88, 5.50, 7.17, 8.84, 10.51, 12.19, and 13.76 kA/m. The arrow indicates the increasing bias magnetic field.

$Fe_{81.4}Ga_{18.6}$ Galfenol rod under various mechanical stresses [19].

Compared with traditional electric motors and hydraulic actuators, magnetostrictive materials are able to provide a high energy density of 1.4–2.5×10^4 J/m^3 while maintaining system stiffness [20]. Magnetostrictive materials react to external magnetic field excitations instantaneously and thus are suitable for dynamic operation. The frequency bandwidth of magnetostrictive actuators is mainly constrained by eddy currents. By creating laminated or particulate magnetostrictive composites, recent magnetostrictive actuators have shown an operating frequency above 20 kHz [21]. Without undergoing permanent depolarization that exists in piezoelectric materials, magnetostrictive materials can also withstand harsh temperature. For instance, the maximum operating temperatures for Terfenol-D and Galfenol are 350 °C and 700 °C, respectively [22, 23]. Due to the magnetically-induced operation, non-contact and wireless operations are possible for rotating machinery and inaccessible structures. Due to the aforementioned merits, magnetostrictive materials have been studied to configure compact and efficient actuators for active vibration control. Magnetostrictive actuators exhibit a frequency response comparable to piezoelectric, electrostatic, or electromagnetic actuators [24]. Unlike their electrically-activated counterparts, magnetostrictive materials operate at dc frequency: a static magnetic

field induces a static and stable response in these materials. Although, in principle, magnetostrictive materials can operate in the tens of thousands of Hertz, in practical actuator systems their response is limited by eddy currents (skin depth effect), electrical inductance, and mechanical resonance [21]. Commercial Terfenol-D-based actuators have been implemented in ultrasonic systems that operate at 20 kHz [25, 26].

2.2. Villari effect

As the mechanical load on the magnetostrictive material increases, all magnetic domains tend to be aligned in the basal plane perpendicular to the load. The domain rotation induces magnetization change, or known as the Villari effect. Figure 3 shows the flux density versus stress curves under various magnetic fields [19].

The stress-induced magnetization variation can eventually generate electrical energy on coils wound around the magnetostrictive materials following Faraday's law. Notable damping coefficients are available by dissipating the electrical energy on a shunt circuit. The Villari effect can also induce significant eddy current loss in electrically-conductive magnetostrictive materials [27, 28]. The stress-induced eddy currents provide a compact damping mechanism that converts mechanical energy to Joule heat without introducing bulky shunt circuits.
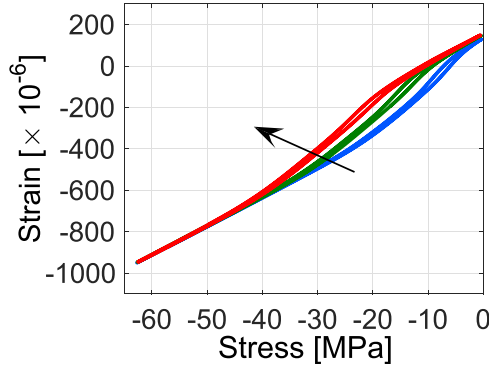
Figure 4. Strain versus stress curves of a $\langle 100 \rangle$-oriented and polycrystalline $Fe_{81.4}Ga_{18.6}$ Galfenol rod. The bias magnetic fields are 2.41, 3.88, and 5.50 kA/m [19]. The arrow indicates the increasing bias magnetic field.
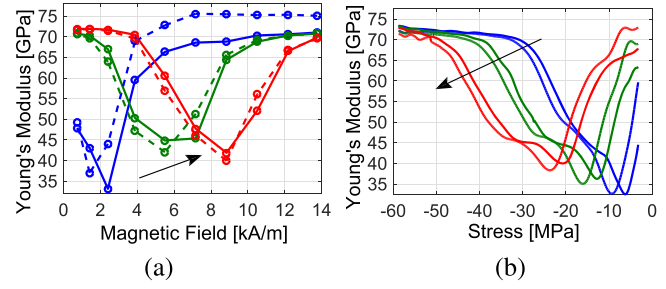

Figure 5. Young's modulus variation of a $\langle 100 \rangle$-oriented and polycrystalline $Fe_{81.4}Ga_{18.6}$ Galfenol rod with respect to (a) a magnetic field of 2.41, 3.88, and 5.50 kA/m and (b) a mechanical stress of -5.73, -27.2, and -41.6 MPa [19]. The arrows indicate the increasing magnetic field and stress.

2.3. Hysteresis

Figure 4 presents typical strain versus stress curves of magnetostrictive materials under various magnetic fields. Due to the material impurities, material anisotropy, and crystal imperfections, magnetostrictive materials exhibit significant hysteresis loss during domain rotation. The hysteresis can be quantitatively described by the area enclosed by the strain versus stress loops. The hysteresis loss has been experimentally characterized for Terfenol-D and Galfenol under different types of magnetic excitations and stress amplitudes [29]. Constitutive models describing the nonlinear hysteresis have been developed and validated in previous studies [30]. Hysteresis presents chanllenges for actuator development; it also provides an intrinsic damping effect that can be beneficial for vibration attenuation.

2.4. Delta-E effect

The strain versus stress curves of Galfenol, shown in figure 4, are nonlinear due to additional magnetostriction. The Young's modulus E of a magnetostrictive material, which is the inverse of the slope of the strain versus stress curve, is estimated by piecewise linearization as

$$E(H, T) = \frac{T}{S_e + \lambda(H, T)}. \tag{1}$$

Here, H and T are the uniaxial magnetic field and stress, respectively; the total strain is the superposition of the elastic strain S_e and magnetostriction λ. Figure 5 shows the nonlinear Young's modulus of a polycrystalline $Fe_{81.4}Ga_{18.6}$ Galfenol sample under various magnetic fields and mechanical stresses. The value of E is stress- and field-dependent. The Delta-E effect, or the change in quasi-static Young's modulus with respect to external excitations, has been documented for Terfenol-D [16, 31–34] and Galfenol [19, 35–39]. The varying Young's modulus can be implemented in active or semi-active vibration isolation.
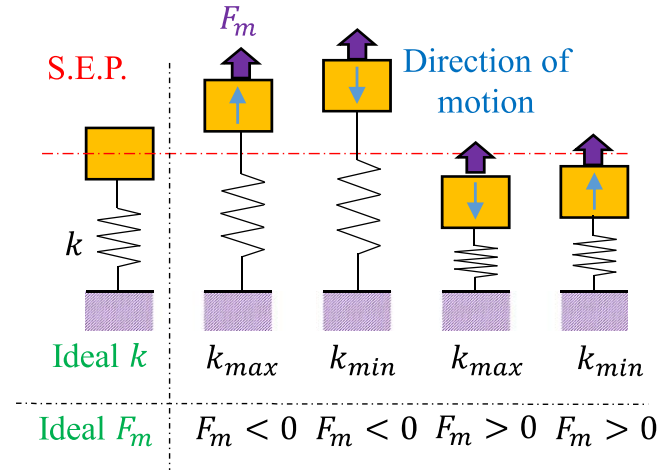
Figure 6. Lumped parameter model for active vibration compensation [40]. The blue arrow indicates the motion of the moving mass; the solid purple arrow indicate the actuation force F_m.

3. Theory

3.1. Vibration compensation

Active vibration compensation mechanisms directly generate a force or continuously adjust system stiffness to act against external disturbances or adjust system stiffness, as illustrated in figure 6. For vibration compensation, the actuation force F_m should be negative when the mass is above the equilibrium position. Otherwise, $F_m > 0$ when the mass is below the equilibrium position. For stiffness tuning, the spring should have a large stiffness k_{max} when the mass moves away from the equilibrium position, while the spring takes a small stiffness when the mass moves towards the static equilibrium position (S.E.P.).

3.2. Frequency tuning

As the frequency of external excitation coincides with one of the system's natural frequencies, resonance occurs. In mechanical systems, resonance is associated with extremely large strain energy and thus can lead to system failure. To avoid resonance, figure 7 shows a frequency tuning mechanism whose natural frequencies can be tuned by changing m
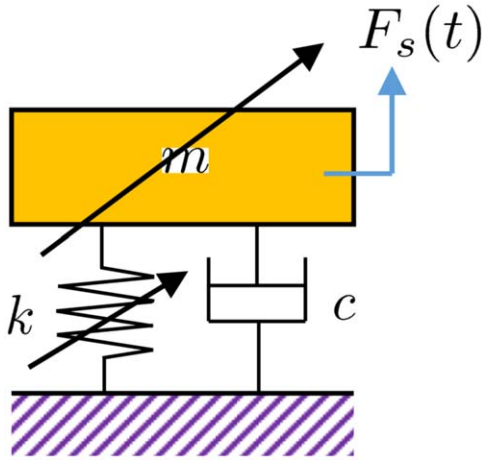
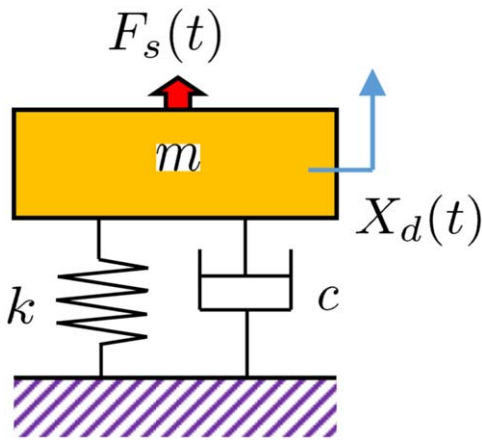**Figure 7.** Lumped parameter model for frequency tuning.

Figure 8. Lumped parameter model for structural damping.

Figure 9. Time-domain responses under a unit impact excitation ($F_s(t) = \delta(t)$) for under-damped ($\zeta = 0.1$), critically-damped ($\zeta = 1$), and over-damped ($\zeta = 2$) systems. ($m = 1$ kg and $k = 4\pi^2$ N · m).

Figure 10. Lumped parameter model for (a) source vibration isolation and (b) base vibration isolation.

or c. In most cases, the mass cannot be easily changed. For example, the mass of a flywheel is determined by the energy storage requirement [1]. Hence, frequency tuning in practice is often equivalent to stiffness tuning.

3.3. Structural damping

Accurate positioning systems (e.g., antennas, microscopes) should be able to resist external impact excitations, such as a gust of wind. The lumped parameter model is presented in figure 8, in which the transfer function is written as

$$T_a(s) = \frac{X_d}{F_s}(s) = \frac{1}{ms^2 + cs + k}, \tag{2}$$

where X_d is the corresponding displacement due to an impact excitation $F_s(t)$. The transfer function can be normalized as

$$T_a(s) = \frac{1}{m} \frac{1}{s^2 + 2\omega_n \zeta s + \omega_n^2}, \tag{3}$$

where the fundamental radial frequency is $\omega_n = \sqrt{k/m}$ and $\zeta = 0.5c/\sqrt{mk}$ is the damping ratio.

Figure 9 shows the impact response of under-damped, critically-damped, and over-damped systems. The vibration amplitude reduces with respect to increasing damping ratio. In
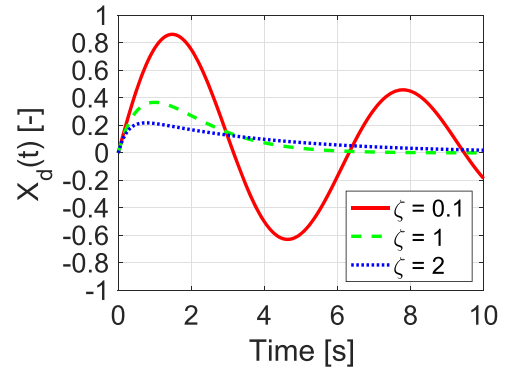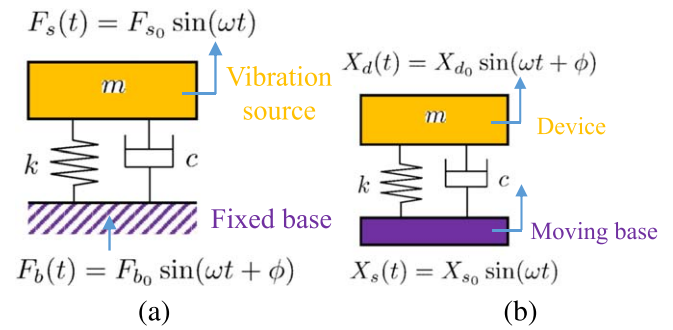
practice, the large damping ratio is typically provided by viscoelastic or superelastic materials. However, these passive damping materials exhibit relative low stiffness and thus dramatically reduce the system resonant frequency. Rigid dampers with large loss factors that can be directly installed in the load path are desirable for future applications.

3.4. Vibration isolation

Figure 10 presents two different configurations of vibration isolators. The first configuration, shown in figure 10(a), reduces the force transmitted from the vibration source $F_s(t)$ to the primary structure. The other configuration, shown in figure 10(b), protects the primary structure from base vibrations $X_s(t)$. The performance of the vibration isolators is described by the force or displacement transmissibility $T_I(s)$, where

$$T_I(s) = \frac{F_b}{F_s}(s) = \frac{X_b}{X_s}(s) = \frac{cs + k}{ms^2 + cs + k}. \tag{4}$$

Here, m is the system mass; F_b and X_d are the force and displacement transmitted to the primary structure,
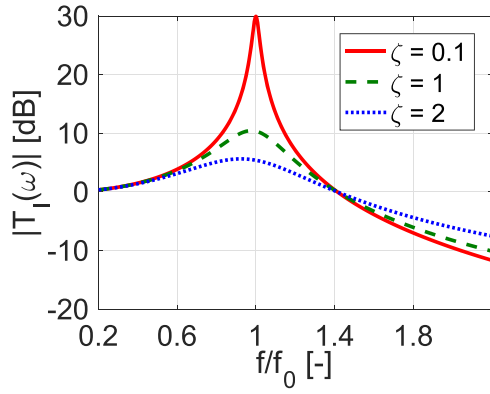
Figure 11. Amplitude of the transmissibility transfer function $|T_I(\omega)|$ with respect to normalized excitation frequency f/f_0, where $f_0 = \omega_n/2\pi$. ($m = 1$ kg and $k = 4\pi^2$ N/m).
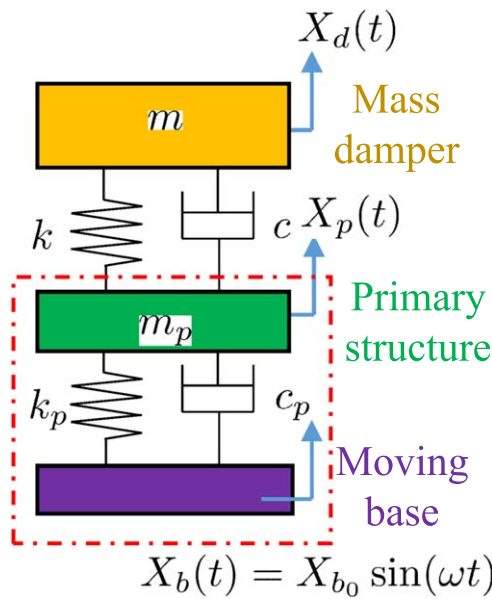

Figure 12. Lumped parameter model for a damped vibration absorber.

respectively. The normalized expression for $T_I(s)$ is

$$T_I(s) = \frac{2\omega_n \zeta s + \omega_n^2}{s^2 + 2\omega_n \zeta s + \omega_n^2}. \tag{5}$$

Figure 11 shows the amplitude of the transmissibility transfer function $|T_I(\omega)|$ with respect to varying excitation frequencies. When the excitation frequency is near DC, $|T_I(\omega)| = 1$. Thus, the stiffness k should be as soft as possible. However, a soft spring may not able to provide enough support. The effect of damping ratio is also presented in figure 11. Under-damped ($\zeta = 0.1$), critically-damped ($\zeta = 1$), and over-damped ($\zeta = 2$) conditions are investigated. A large damping reduces $|T_I(\omega)|$ around the system resonance but degrades the performance at high frequencies. Hence, the values of k and c need to be selected accordingly based on the desired system response [11].
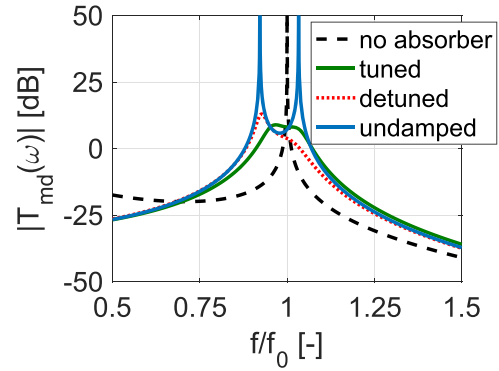
Figure 13. Amplitude of the displacement transmissibility $|T_{md}(\omega)|$ with respect to normalized excitation frequency for a 2nd order system, where $m = 1$ kg, $m_p = 100$ kg, $k_p = 400\pi^2$ N/m, and $c_p = 0.05$. (black: no vibration absorber; blue: undamped vibration absrober; green: tuned and damped vibration absorber; red: de-tuned and damped vibration absorber when the resonance of the primary structure reduces by 5%).

3.5. Vibration absorption

The damped vibration absorber presented in figure 12 is able to suppress the resonance of the primary structure. The displacement transmissibility between the base excitation X_b and the vibration of the primary structure X_p is

$$T_{md}(s) = \frac{X_p}{X_b}(s) = \frac{c_p s + k_p}{DEN(s)}, \tag{6}$$

where

$$DEN(s) = mm_p s^4 + (cm + cm_p + c_p m)s^3$$
$$+ (cc_p + km + km_p + k_p m)s^2 + (k_p c + kc_p)s + kk_p. \tag{7}$$

Here, the subscription p denotes the primary structure. Optimal stiffness k_{opt} and damping coefficient c_{opt} have been selected empirically for harmonic excitations following [41], where

$$k_{opt} = \frac{mm_p^2 \omega_n^2}{(m + m_p)^2},$$

$$c_{opt} = m\sqrt{\frac{3k_{opt}}{2(m + m_p)}}. \tag{8}$$

Figure 13 presents the displacement transmissibility of a 2nd order system. The tuned vibration absorber designed following equation (8) is able to reduce the transmissibility amplitude around the system's resonance. When the resonant frequency of the primary structure reduces by 5%, the performance of the vibration absorber deteriorates dramatically. The parameters of the vibration absorber are preferred to be adjustable to follow the system variations.

4. Vibration control

Due to the unique material properties discussed in section 2, magnetostrictive materials have been widely investigated in
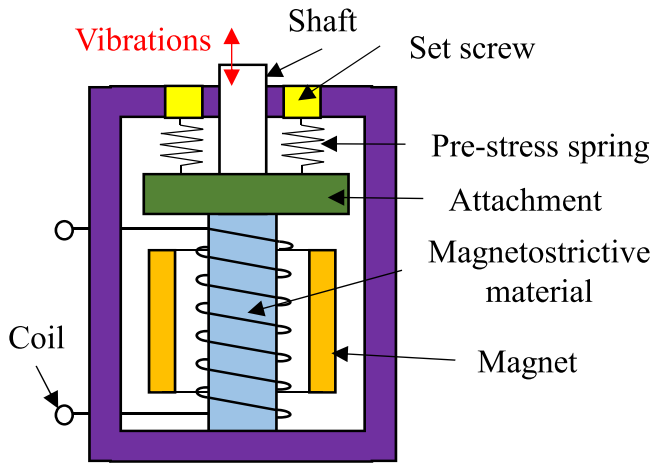
Figure 14. Schematic of a magnetostrictive actuator.

structural vibration control. This section reviews the current state of magnetostrictive materials in active, passive, and semi-active vibration control.

4.1. Active vibration control

Taking advantage of the Joule magnetostriction, previous studies have developed magnetostrictive actuators that are able to generate dynamic forces or motions to counteract external vibrational disturbance. Figure 2 shows that the deformation of magnetostrictive materials is maximized when they operate around the center of the burst region or when the input mechanical energy balances with the magnetic energy. To maximize the stroke, figure 14 shows a typical configuration of a magnetostrictive actuator. The bias stress is usually applied by a pre-stress spring or Belleville washer. The bias magnetic field is applied by a DC current through the solenoid [42]. In practice, the bias magnetic field can also be generated by a cylindrical permanent magnet to avoid head build up as is the case with DC currents.

The effectiveness of active control strategies depends on how the magnetostrictive actuators are integrated with the primary structure. Various actuator placement strategies have been studied for helicopter struts to attenuate longitudinal and flexural vibrations transmitted from main gearbox to the fuselage. As shown in figure 15, Mahapatra et al [43] proposed four different actuator configurations. The performance of each configuration was validated numerically by theoretically designing a feedback control algorithm together with an active spectral element model. The serial configuration, in figure 15(a), can achieve considerable reduction in longitudinal vibrations throughout the frequency range of interest [44]. By orienting the magnetostrictive actuator perpendicular to the strut, as shown in figure 15(b), the flexural vibration waves can be significantly attenuated. Figure 15(c) proposes a hybrid configuration targeting the coupled longitudinal-flexural vibrations. Magnetostrictive actuators in figures 15(a) and (c) have to be placed in the load path and thus may not be feasible in practice. Thus, an alternate, shown in figure 15(d), implements a pair of magnetostrictive actuators in parallel to
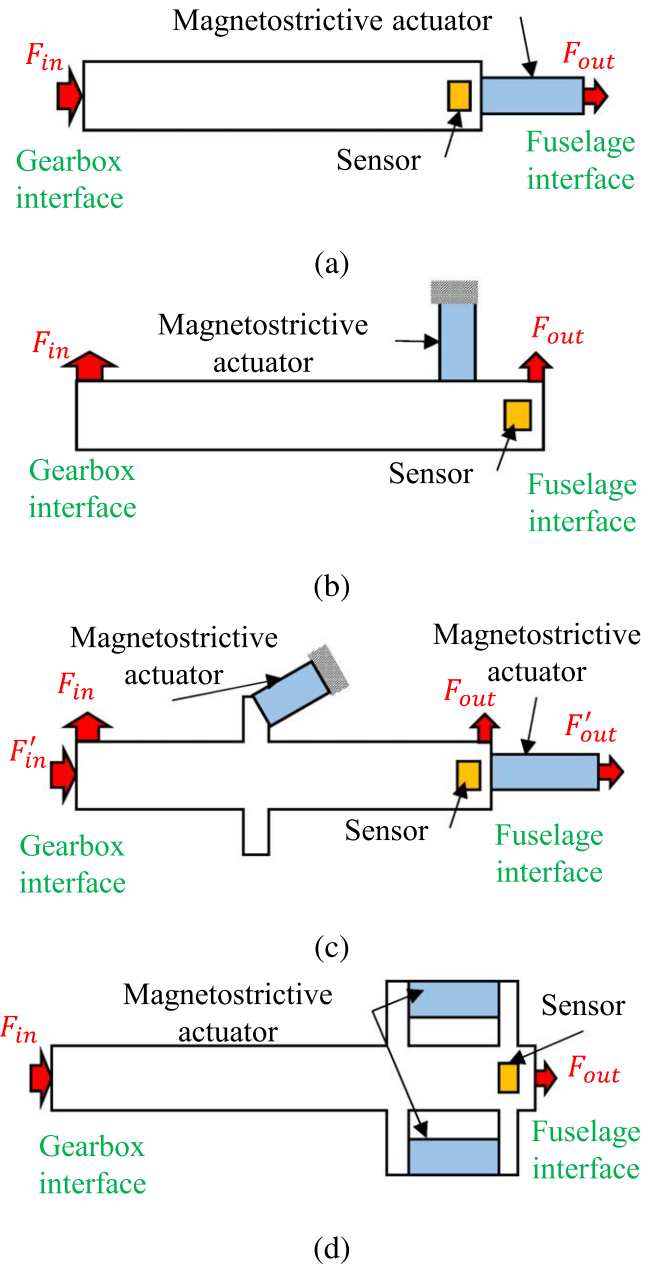

Figure 15. Placements of magnetostrictive actuators in helicopter struts: (a) serial orientation, (b) vertical orientation, (c) hybrid orientation, and (d) parallel orientation [43].

attenuate longitudinal vibrations. The parallel configuration has been validated experimentally.

Sutton et al [45] placed three actuators in parallel to a helicopter gearbox support strut, as shown in figure 16. By driving the three actuators in phase, the active strut attenuated by 30–40 dB the kinetic energy measured on the fuselage connection side over a frequency range of 250–1250 Hz. Attenuation in flexural wave transmission is possible by driving the three actuators out-of-phase.

Similar to the vertical orientation proposed in figure 15(c), several experimental studies have been conducted to suppress flexural vibrations. As shown in figure 17, Pratt et al [46] installed a Terfenol-D actuator at the base of a cantilever beam. A feedback control loop was designed to
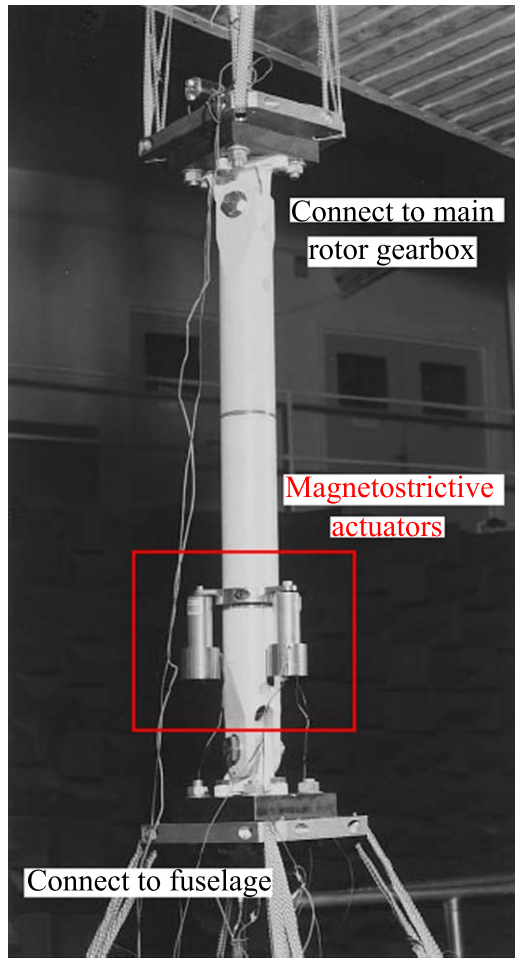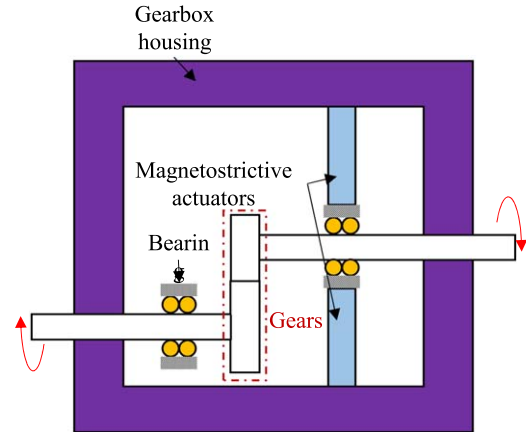
Figure 16. Active helicopter strut with three parallel oriented magnetostrictive actuators [45].
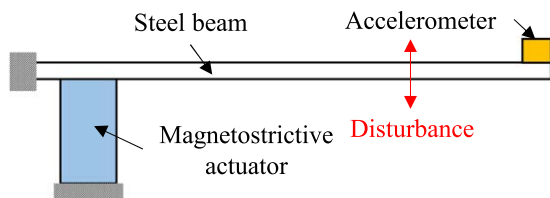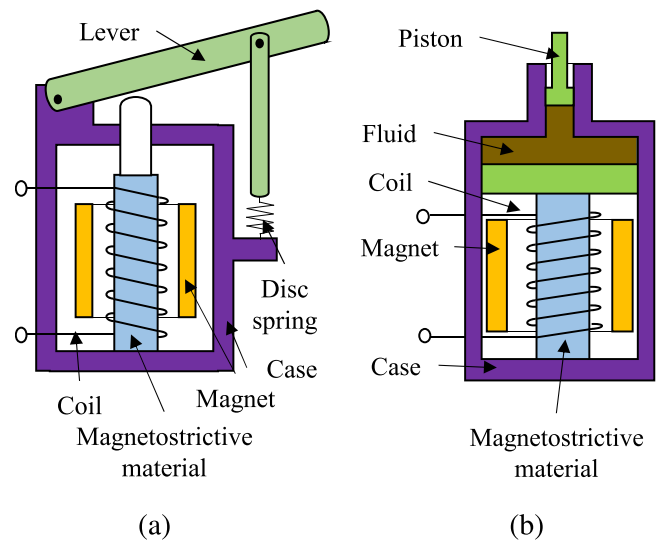

Figure 17. Magnetostrictive actuator configuration to attenuate flexural vibrations in a cantilever beam [47].


Figure 18. Gearbox with two pairs of magnetostrictive actuators supporting the bearing [49].

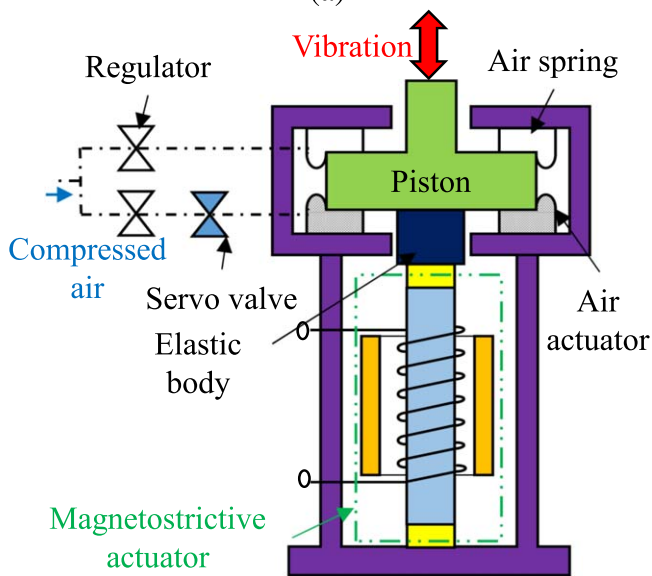
Figure 19. Hybrid magnetostrictive actuators incorporated with (a) a lever mechanism [51] and (b) a hydraulic cylinder [53].

attenuate the tip acceleration induced by the external disturbance applied in the middle of the beam. The actuator was controlled to suppress the first and second modes. Utilizing a similar experimental setup, Flatau *et al* [47] actively drove a Terfenol-D actuator such that its deformation amplitude was proportional to the tip acceleration and its phase was 180° out-of-phase. The simple controller attained a −23 dB reduction in tip acceleration at frequencies up to 4 kHz. Theoretical analysis presented a frequency limit of more than 10 kHz. Moon *et al* [48] implemented a pair of Terfenol-D actuators to support both ends of a simple aluminum beam. Together with a linear quadratic feedback controller, the active vibration control was able to reduce the flexural

vibrations by 12–20 dB up to a frequency of 500 Hz suppressing the first four modes of vibrations.

Besides helicopter gearbox struts, magnetostrictive actuators have been applied to attenuate vibrations induced by gear meshing. Rebbechi *et al* [49] configured four Terfenol-D actuators distributed circumferentially around a rotating shaft, as shown in figure 18. Two actuators were normal to the contact point of the meshing gears. The other pair was installed perpendicular to the first pair. Each pair of actuators was driven 180° out-of-phase and operated in push-pull mode. Both the acceleration on the gearbox housing and the sound pressure outside of the gearbox were measured. By simultaneously minimizing the first three modes of the gear pair via an adaptive feedforward controller, the acceleration amplitude was reduced by 20–28 dB, 5–10 dB, and 0–2 dB for 1×, 2×, and 3× of the gear mesh frequency, respectively. Guan *et al* [50] later proposed several actuator configurations to attenuate gear pair vibrations using less number of actuators.
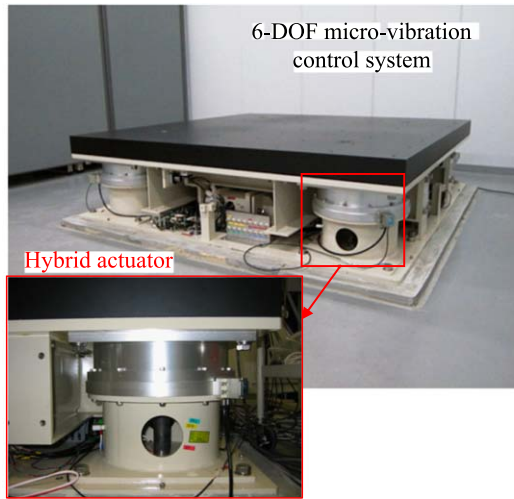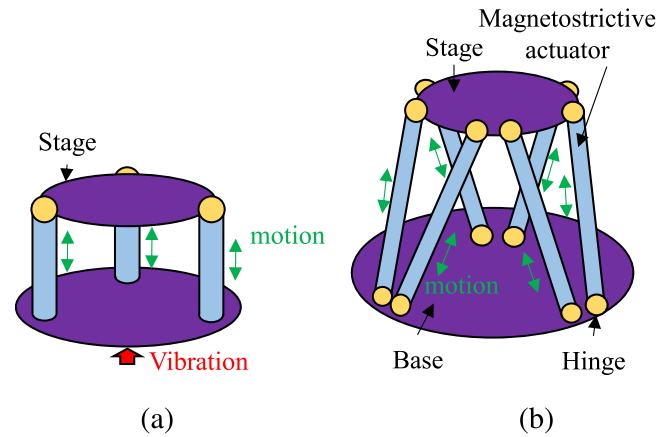
Figure 20. (a) Physical assembly and (b) schematic of magnetostrictive-air hybrid actuator [56].

Figure 21. (a) 3-DOF vibration isolation table [57] and (b) 6-DOF Stewart platform [58].

Magnetostrictive actuators exhibit a large energy density but a relatively small stroke. For vibration control systems that requires large deformation, hybrid actuators have been developed. Bartlett *et al* [51] combined a lever mechanism with a Terfenol-D actuator, as shown in figure 19(a). Two Terfenol-D rods (Φ30 mm by 254 mm long) were connected in series. With a lever gain of 6, the hybrid actuator generated a maximum displacement of 4 mm and an associated zero-displacement force of 0.5 kN. This actuator is only suitable for civil engineering structures (e.g., bridge cables) due to its narrow frequency bandwidth. Vibrations in automobile systems span a much wider frequency range. For instance, the engine vibrations ranges from 20 Hz to 400 Hz, depending on the number of cylinders, the engine speed, and the stroke number [52]. Commercial electrodynamic engine mount actuators can provide a stroke in the millimeter range with a narrow frequency range up to 110 Hz [53]. Chakrabarti and

Dapino [53–55] incorporated a hydraulic cylinder with a Terfenol-D actuator, as shown in figure 19(b). The hybrid actuator is able to improve the maximum frequency to 280 Hz while meeting the displacement requirement and lowering the power consumption. Nakamura *et al* [56] developed another hybrid actuator combining an air actuator and a Terfenol-D-based actuator, as shown in figure 20. The air actuator has a relatively large displacement in the low frequency range, while the magnetostrictive actuator is able to provide significant displacement at high frequencies.

By arranging several actuators in particular patterns, multiple degrees of freedom (DOFs) vibration control platforms have been developed. Bryant *et al* [57] installed three Terfenol-D actuators in parallel, as shown in figure 21(a), and the performance of the 3-DOF vibration isolation platform was evaluated by measuring the vibration power transmitted from the base to the stage. For a 70 Hz base excitation, a PID controller and a neural network controller attenuated the vibration power by 6.9 dB and 15 dB, respectively. Geng and Haynes [58] designed a 6-DOF Stewart platform to reduce vibrations in space structures, as shown in figure 21(b). At the resonant frequency of 62.4 Hz, the adaptive filter controller achieved a 30 dB vibration attenuation. Nakamura *et al* [56] implemented 8 air-magnetostrictive hybrid actuators to construct a micro-vibration isolation table, as shown in figure 20(a), where 4 of them are aligned vertically and the rest 4 are oriented horizontally. The performance of the isolation table has been experimentally validated to isolate floor vibrations for a focused ion beam (FIB) image machine [59, 60].

Patterned magnetostrictive actuators can also provide large actuation power for civil engineering applications. Fujita *et al* [61] replaced the existing current-active vibration absorbers by 32 magnetostrictive actuators to actively attenuate seismic vibrations in a three-story building. A 15% modal damping ratio was achieved up to the 3rd mode of the structure.

Most of the existing studies utilized Terfenol-D-based actuators, which exhibit low tensile strength and require special protection mechanisms. Flexible magnetostrictive
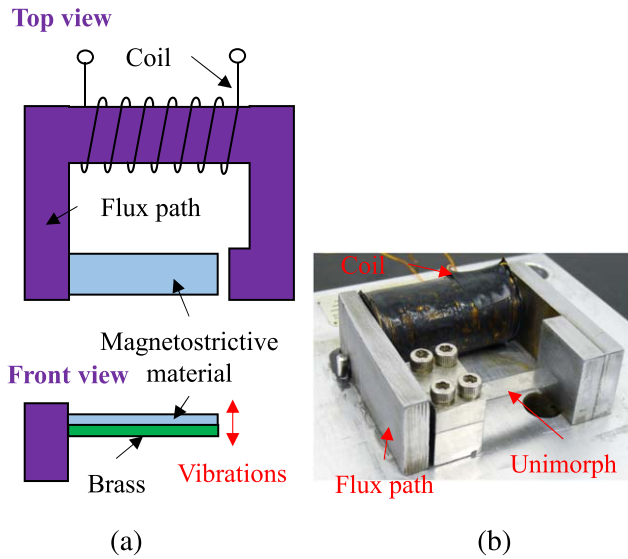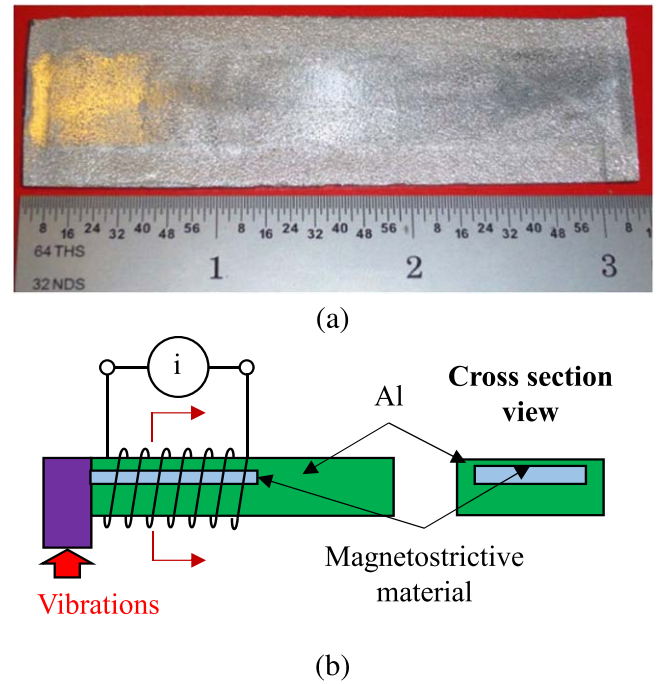
Figure 22. (a) Schematic and (b) physical assembly of a magnetostrictive unimorph actuator.

Figure 23. (a) Magnetostrictive composites with embedded Galfenol inside Al 3003 base structure using ultrasonic additive manufacturing (UAM); (b) unimorph actuator based on UAM-ed magnetostrictive composites [65].

Figure 24. Three magnetostrictive actuator driven inertia masses mounted on a gear body [68].
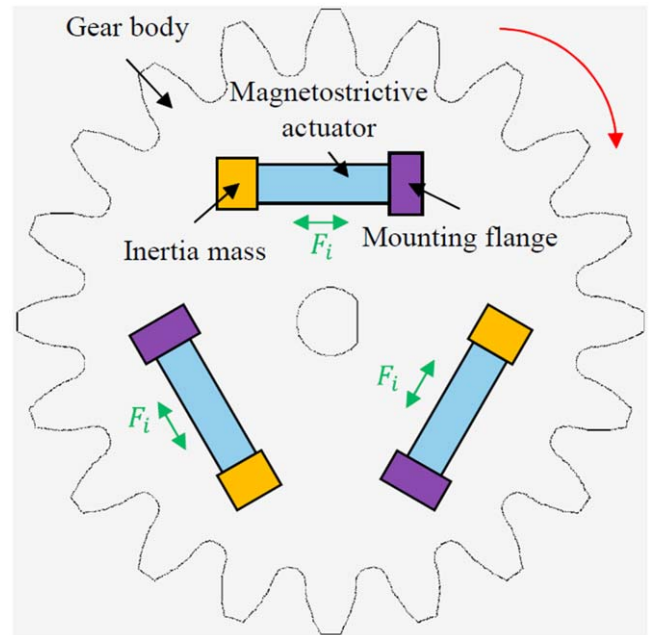
actuators have been developed by embedding magnetostrictive particles into resins. Murty *et al* [62] created a laminated composite beam that contains a Terfenol-D particle embedded layer. Zhou and Zhou [63] later implemented a negative velocity feedback controller together with an analytical nonlinear constitutive model to mitigate the composite beam vibrations. Due to the large actuation force enabled by the Terfenol-D composite layer, this numerical study demonstrated a maximum effective damping factor of about 0.09.

Limited by the volume fraction of Terfenol-D particles, the magneto-mechanical coupling in magnetostrictive composites is dramatically weaker than that in the monolithic magnetostrictive materials. Taking advantage of mechanically-robust Galfenol, Shu *et al* [64] fabricated a unimorph composite beam by bonding a Galfenol layer on a nonmagnetic substrate, as shown in figure 22. A finite-dimensional sliding-mode controller was developed to accurately control the tip deflection to 400 Hz. The bending motion can effectively amplify the deformation of the magnetostrictive layer, but the super glue utilized to bond the unimorph degrades the reliability [64]. To improve the mechanical strength and corrosion resistance of the unimorph composites, Scheidler and Dapino [65] utilized ultrasonic additive manufacturing to encapsulate magnetostrictive Galfenol within aluminum structures, as shown in figure 23. Magnetostrictive materials have low inherent structural damping and will induce instability when an error occurs in feedback control. Bhattacharya *et al* [66] and Bandopadhya *et al* [67] combined the magnetostrictive composite actuator with passive damping materials (e.g., poly-ethylene glycol, Fe-Cr-Al alloys) to achieve distributed control of vibrations.

Besides direct force compensation, the actuation force can be generated indirectly via driving inertia masses at high frequencies. As shown in figure 24, Chen and Brennan [68]

mounted three magnetostrictive actuators with tip inertia masses on a gear body. The inertia force successfully damped out the gear angular vibrations by 7.5 dB at the tooth meshing frequency around 250 Hz. However, this configuration induced mass imbalance. The inertia actuator cannot attenuate low frequency vibrations, since the inertia force is relatively small at low frequencies.
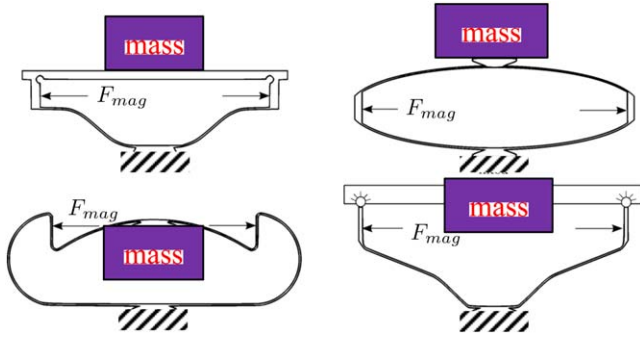
Figure 25. Flexure mechanisms for low frequency inertia force generation.
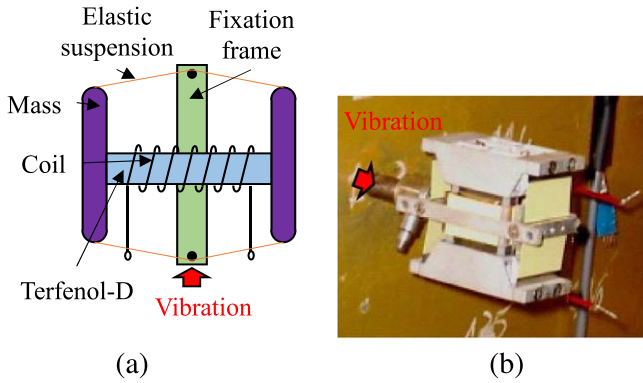
Figure 26. (a) Schematic of a magnetostrictive flexure actuator and (b) a magnetostrictive flexure actuator mounted on a fuselage skin panel of a Boeing 717 [72].

Figure 27. (a) Computer-Aided Design (CAD) drawing and (b) physical assembly of magnetostrictive variable spring [73].

Braghin *et al* [69] numerically studied the four flexure mechanisms presented in figure 25, where the small elongation of the magnetostrictive material and the resulting small inertia force are significantly amplified. Experimental results shows that the flexure mechanism is able to achieve a large inertia force down to 167 Hz. As shown in figure 26, May *et al* [70] enclosed a magnetostrictive actuator inside a flexure cage, which was mounted on the fuselage of a turboprop aircraf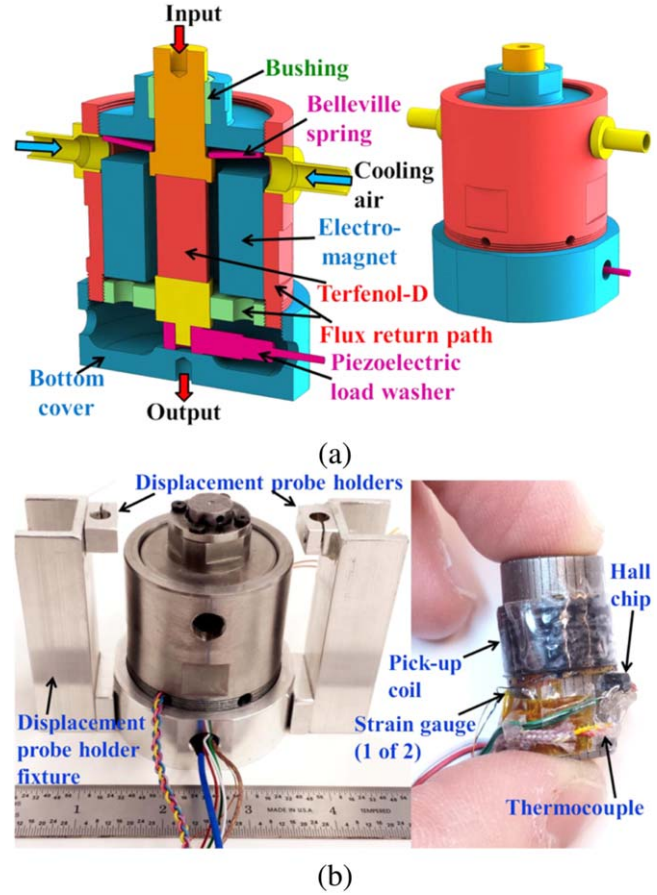t. It can attenuate the vibration tones generated by the propeller at the fundamental blade passage frequency and its harmonics. The anti-resonance of the actuator provide an vibration attenuation of 12 dB. Aurilio *et al* [71] later designed a multi-input-multi-output feedback controller for the actuator and attained 15–50 dB vibration attenuation between 40 and 200 Hz. Cavallo *et al* [72] connected a fiber Bragg grating sensor in parallel to the magnetostrictive actuator to create a low-level control loop that compensates the nonlinear behavior of the magnetostrictive actuator. Within a frequency range between 150 and 400 Hz, an average 14.4 dB vibration reduction was obtained experimentally from an actual aircraft fuselage skin shown in figure 26(b).

In addition to the Joule magnetostriction that generates a force or a displacement counteracting the external disturbances, the Delta-E effect of magnetostrictive materials provides another actively vibration control strategy by tuning system stiffness. Scheidler *et al* [73] developed a variable

spring, as shown in figure 27, whose stiffness can be actively controlled by tuning the current through the electromagnet. A peak-to-peak sinusoidal Young's modulus variation of 21.9 GPa was achieved up to 500 Hz. The maximum peak-to-peak Young's modulus for a square wave switch was 12.3 GPa. A numerical simulation of this device demonstrated an effective loss factor of 0.13 [40].

4.2. Passive control

The damping capacity of magnetostrictive materials is usually described by the loss factor η in previous studies [15, 74]. The value of η is calculated from strain versus stress curves as

$$\eta = \tan(\phi_{TS}), \tag{9}$$

where ϕ_{TS} is the phase lag between the strain and stress. Bozorth [75] demonstrates two energy dissipation mechanisms in ferromagnetic materials: magnetic hysteresis and eddy currents.

Following Bozorth's theory, the magnetic hysteresis is constant up to the characteristic frequency of the magnetic system (f > 1 MHz) [76]. The magnetic hysteresis of polycrystalline Galfenol (at 18.4% Ga) was characterized by Restorff *et al* [29], which is not significant enough for passive damping. Hathaway *et al* [76] observed a loss factor of 0.29 from the hysteretic strain versus stress loops of Terfenol-D.

The damping effect of Terfenol-D relies on material composition, crystal structure, and fabrication method. Hathaway *et al* [76] qualitatively showed the trend of loss factor with respect to material anisotropy using an analytical model. Teter *et al* [77] experimentally investigated the damping capacity of Terfenol-D with respect to different micro structures. The loss factors of polycrystalline Terfenol-D ($Tb_{0.3}Dy_{0.7}Fe_2$) and eutectic Terfenol-D ($Tb_{0.6}Dy_{0.4}Fe_{1.4}$) samples fabricated by free-standing zone melt (FSZM) method were characterized under no magnetic field. The eutectic sample exhibits a stress-independent loss factor of about 0.04; the loss factor of polycrystalline Terfenol-D varies with respect to stress amplitude and reaches a maximum value of 0.28 at 4.1 MPa. Wun-Fogle *et al* [78] experimentally investigated the damping capacity of FSZM-fabricated Terfenol-D ($Tb_xDy_{1-x}Fe_{1.92}$) as a function of the terbium content x. A maximum loss factor of 0.22 was observed for $x = 0.45$ under 23.9 kA/m bias field. Ho *et al* [79] measured the damping capacity of Terfenol-D ($Tb_xDy_{1-x}Fe_{1.92}$) fabricated by arc-melt method for x varies from 0.35 to 1.0. A maximum loss factor of 0.15 was achieved at $x = 0.5$ under a magnetic field of 23.9 kA/m. The optimal x is similar to the monolithic FSZM samples, but the loss factor is much smaller.

To resolve the brittleness of monolithic Terfenol-D, Sandlund *et al* [80] embedded Terfenol-D particles into insulating binders and created flexible magnetostrictive particulate composites (MPC). Ho *et al* [79] experimentally compared the loss factors of MPC that are made of Terfenol-D particles fabricated by FSZM and arc-melt. Unlike the results from the monolithic samples, MPC based on arc-melt Terfenol-D particles exhibit a higher loss factor than that of the FSZM-fabricated MPC. The arc-melt MPC is able to provide a maximum loss factor of 0.09 while maintaining a high Young's modulus of about 10 GPa. Pulliam *et al* [81] later applied a thin layer of MPC on top of a turbomachinery fan blade and achieved a 35% increment in structural damping.

The other energy dissipation mechanism associated with magnetostrictive materials is the stress-induced eddy currents. Deng [27] and Scheidler and Dapino [28] have developed analytical constitutive models describing the eddy current loss in magnetostrictive materials. Scheidler *et al* [82] experimentally characterized the eddy current loss up to 1 kHz by comparing the strain versus stress curves measured from a solid and a laminated Galfenol sample ($\Phi 6.35$ mm). Deng *et al* [83] later conducted a parametric study for a solid-state damper where the active component is a 6 mm diameter and 10 mm long Galfenol rod. The proposed damper was validated experimentally by Deng *et al* [84], which demonstrated a maximum loss factor of 0.05 at 1 kHz.

The stress-induced eddy current loss depends on the device's geometry. To create significant damping for arbitrary geometries, recent studies have incorporated a shunted circuit with the magnetostrictive materials, as shown in figure 28. Due to the Villari effect, mechanical stress induces magnetization variation inside magnetostrictive materials and generates electrical energy in the coil. The vibration energy is
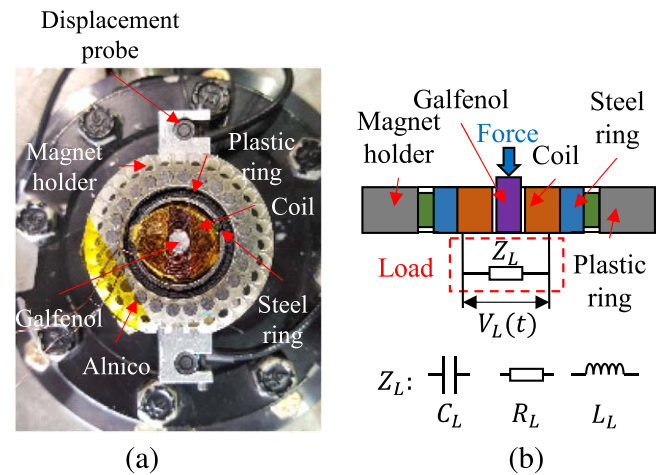

Figure 28. (a) Schematic and (b) physical assembly of magnetostrictive unimorph [84]. (C_L: capacitive shunt; R_L: resistive shunt; L_L: inductive shunt).
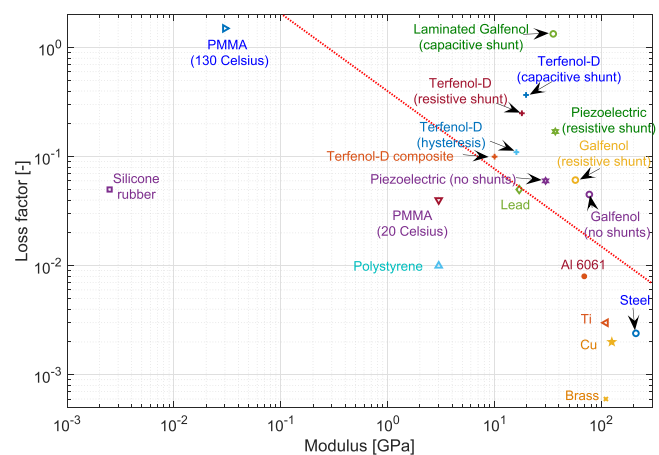
Figure 29. Loss factor versus Young's modulus map. PMMA: polymethylmethacrylate; Terfenol-D: $Tb_{0.3}Dy_{0.7}Fe_2$; Galfenol: $\langle 100 \rangle$-oriented polycrystalline $Fe_{81.6}Ga_{18.4}$; Piezoelectric: Noliac NCE51F, soft-doped polycrystalline PZT.

eventually dissipated on the electrical shunt as joule heat. Davino *et al* [85] measured the damping capacity of a shunted Galfenol damper via impact testing. However, the bias magnetic field in this device was applied via an electromagnet requiring external power supply. Deng *et al* [84] experimentally characterized the loss factor available from this shunted damper which was biased by permanent magnets. At 750 Hz, the maximum loss factors from a Galfenol-based shunted damper are 0.06 and 1.34 for resistive shunt and capacitive shunt, respectively. Asnani *et al* [15] measured the loss factor of a Terfenol-D damper and achieved a maximum loss factor of 0.25 at 300 Hz for resistive shunts. Fenn and Gerver [86] developed a Terfenol-D-based shunted damper which simultaneous operates as a velocity sensor. A maximum loss factor of 0.22 and a velocity sensitivity of 180 V/(m/s) were measured. Figure 29 compares the loss factor and Young's modulus of magnetostrictive materials and other industrial passive damping materials. Magnetostrictive
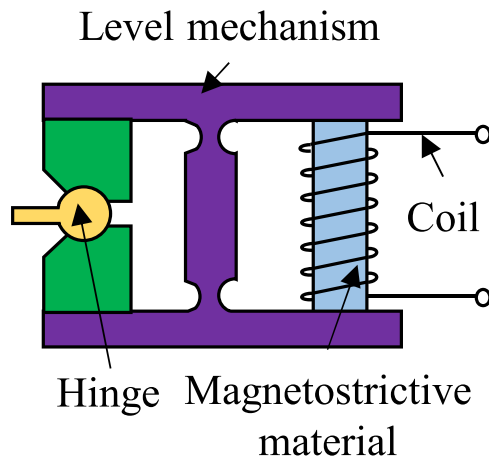
Figure 30. Active hinge that incorporates the magnetostrictive actuator with lever mechanisms [88].

materials are ideal candidates for structural damping applications when high stiffness is desirable.

Magnetostrictive materials are usually appropriate for small vibration amplitude and high frequencies. Hybrid damping materials based on magnetostrictive materials have been developed to lift these limitations. Kerrigan *et al* [87] fabricated a NiTi/Ni/Terfenol-D laminated composite. The NiTi film dissipates vibration energy for low frequency and large strain amplitudes; the Terfenol-D film manufactured by sputter deposition targets the high frequency vibrations. Overall, the hybrid damper is feasible for a wide strain range from 0.05% to 1%. A maximum loss factor of 0.21 is achieved at 0.27% strain.

4.3. Semi-active control

Semi-active vibration control that requires minimum control effort or energy consumption has been investigated in recent applications. The first type of semi-active control is to integrate traditional magnetostrictive actuators with passive mechanisms. Ohmata *et al* [88] developed a smart joint, shown in figure 30, whose hinge friction increases as the magnetostrictive rod elongates. Figure 31 shows another semi-active mechanism that mitigates higher harmonics following individual blade control [89]. The semi-active system is able to tilt the edge flap by ±5° while taking less than 1% of the gross vehicle weight and using only 0.7% of cruise power.

Section 4.1 presented several actuators that can actively generate time-varying inertia forces to compensate external disturbance. However, the real-time actuation requires complicated controllers and distributed sensors. Semi-active vibration absorbers that utilize DC driving currents have been developed in the literature to reduce the control complexity. Flatau *et al* [90] designed a Terfenol-D-based vibration absorber whose resonant frequency was tuned by applying different DC currents through the solenoid. The anti-resonance introduced by the vibration absorber shifted from 1375 Hz to 2010 Hz by applying a current of 2 A. Braghin *et al* [91] configured a similar device and developed
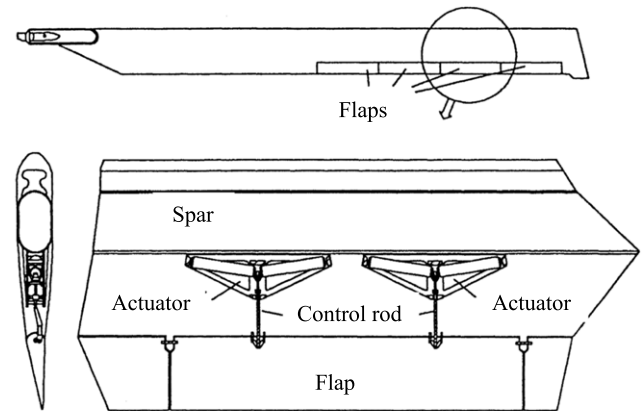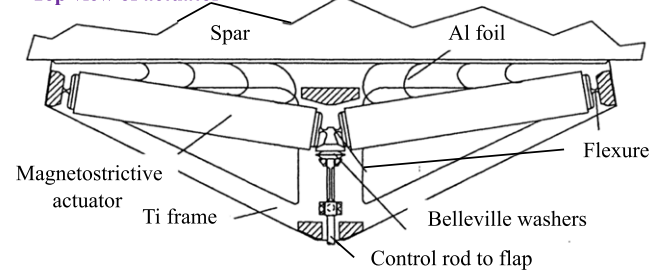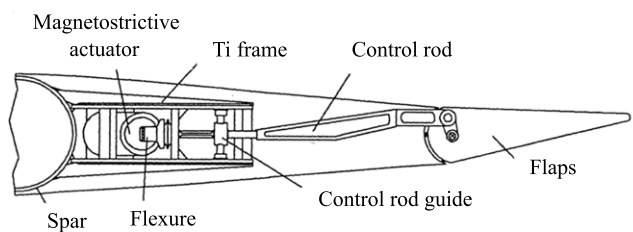
Figure 31. (a) Arrangement of magnetostrictive actuators and trailing edge flaps for the UH-60A helicopter blades; (b) Top and aft view of the magnetostrictive actuator linked to flap [89].

a lumped parameter model to describe the current-induced resonance tuning.

Other semi-active vibration control mechanisms can be developed by modifying the aforementioned active and passive control strategies. As shown in figure 27, the stiffness of magnetostrictive materials can be actively controlled by applying a suitable current to the solenoid. Recent studies demonstrated that the stiffness can also be tuned by attaching various electrical impedances to the coil. Semi-active smart mounts based on Terfenol-D and Galfenol have been developed for the main rotor gearbox of helicopters, as shown in figure 32. Scheidler and Asnani [92] derived a lumped parameter model and conducted parametric studies for the proposed tunable mount based on linearized constitutive models. The Terfenol-D mount and Galfenol mount were experimentally characterized in [93] and [84], respectively. Table 2 summarizes the relative stiffness variation under various electrical impedances.
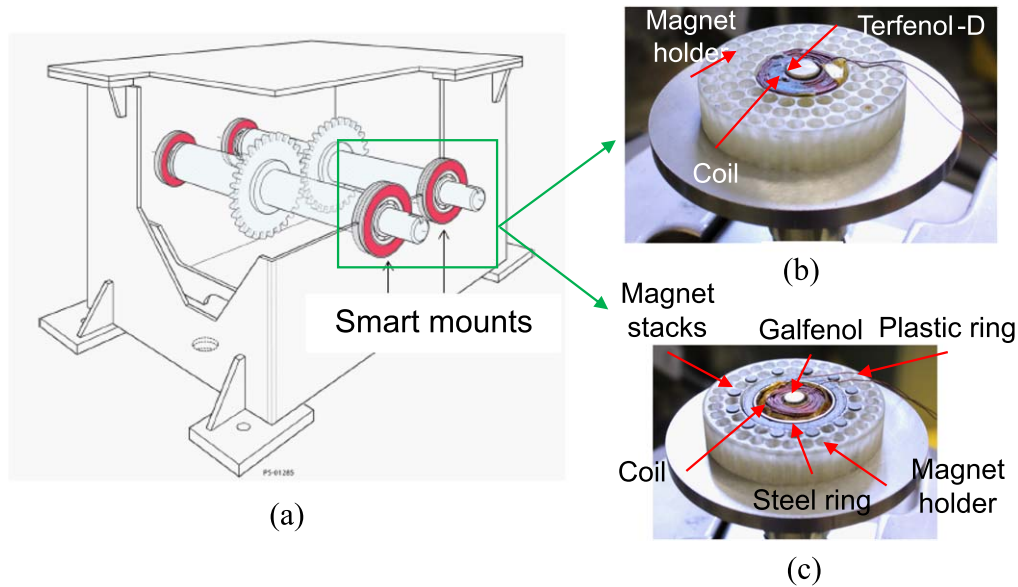
Figure 32. (a) Installation locations of the smart mount in a helicopter main gear box; (b) Terfenol-D-based and (c) Galfenol-based smart mounts.

Table 2. Relative stiffness $\bar{K} = (K_{max} - K_{min})/K_{max}$ measured from solid Terfenol-D (ϕ 7 mm $\times$ 10 mm), solid and laminated $Fe_{81.6}Ga_{18.4}$ Galfenol (ϕ 6 mm $\times$ 10 mm) under various types of electrical shunts. A 750 Hz and 280 N amplitude was applied to the Terfenol-D sample and a 750 Hz and 73.51 N amplitude sinusoidal force was applied to the Galfenol samples.

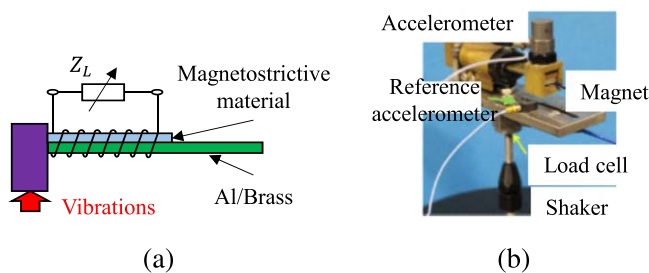| Material	Resistive	Capacitive	Inductive
Terfenol-D	19.5%	24.6%	NA
Solid Galfenol	6.7%	17.9%	6.7%
Laminated Galfenol	11.0%	60.9%	10.9%

Figure 33. (a) Schematic and (b) physical assembly of tunable shunted dampers [94].

Table 3. Loss factor η range measured from solid Terfenol-D (Φ 7 mm $\times$ 10 mm), solid and laminated $Fe_{81.6}Ga_{18.4}$ Galfenol (Φ6 mm $\times$ 10 mm) under various types of electrical shunts. A 750 Hz and 280 N amplitude was applied to the Terfenol-D sample and a 750 Hz and 73.51 N amplitude sinusoidal force was applied to the Galfenol samples.

Material	Resistive	Capacitive	Inductive
Terfenol-D	0.11−0.21	0.21−0.37	NA
Solid Galfenol	0.01−0.05	0.03−0.22	0.01−0.03
Laminated Galfenol	0.01−0.06	0.01−1.34	0−0.01

Section 4.2 demonstrated typical passive magnetostrictive dampers by attaching shunt circuits to magnetostrictive materials. Recent studies have shown that the shunt damper can be tuned by changing the impedance of the electrical shunt. Yoo et al [94] first evaluated the impedance-dependent loss factor of a Galfenol-based unimorph, as shown in figure 33. Deng [93] and Deng et al [84] later characterized the damping capacity of Terfenol-D and Galfenol, respectively, by applying axial mechanical load to the mounts presented in figure 32. The loss factors under various types of electrical impedance are summarized in table 3. Compared with similar shunted dampers based on piezoelectric materials [15], magnetostrictive materials are able to provide a higher loss factor. Due to the mechanical robustness, high stiffness, and large damping capacity of Galfenol, Deng et al [74] recently developed a ring-shaped damper which can be mounted inside gear body and dissipate gear meshing vibrations before they propagate and induce structure-borne noise. The semi-active vibration control devices mentioned above can also be self-sustained, since part of the electrical energy on the shunted circuit can be scavenged [95, 96]. Theoretical results show that larger stiffness variation are available when negative inductive loads is attached [92].

5. Conclusion

The magneto-mechanical coupling in magnetostrictive materials forms the basis for several responses including Joule magnetostriction, Villari effect, magnetic hysteresis, and Delta-E effect. Each of these effects have been shown to prove useful in the design of active, passive, or semi-active vibration control approaches. Many magnetic materials exhibit magnetostrictive behavior, but this article focuses on

two widely-used magnetostrictive materials: Terfenol-D and Galfenol.

Due to the Joule magnetostriction, magnetostrictive materials are able to provide a large actuation stress (MPa level) or moderate strain (0.16%) that can actively counteract external disturbances. Compared to conventional electromagnetic motors, magnetostrictive actuators exhibit a large stiffness and a broad frequency bandwidth. Certain magnetostrictive materials, such as Galfenol or Alfenol, are mechanically-robust and can withstand complex loadings. The magnetostrictive actuators are activated by magnetic field and thus are suitable for wireless or non-contact cases. Monolithic magnetostrictive materials typically have a high electrical conductivity. Hence, the frequency bandwidth of the magnetostrictive actuators is mainly limited by the eddy currents. Lamination or particle embedded composites are common solutions to mitigate the eddy currents. Another limitation of magnetostrictive actuators is their relatively small deformation. To extend the applications of magnetostrictive actuators to large deformation cases, existing studies either fabricate composites (e.g., magnetostrictive unimorph) that converts small elongation to large bending motion or construct hybrid actuators that incorporate lever mechanisms, flexural mechanisms, hydraulic cylinder, or pneumatic systems to amplify the deformation. Magnetostrictive actuators that are installed in the load path can efficiently counteract vibration sources although a disadvantage of this approach is the added complexity. Control force can be applied indirectly through inertia masses. The indirect mechanisms have been developed and experimentally validated to attenuate vibrations on aircraft fuselage and gear bodies. However, the inertia mass introduces additional weight that is undesirable for mobility applications. Adding inertia mass on gear pairs also induces rotating unbalance that can be detrimental to system reliability. Future studies should further explore the potential applications of mechanically-robust magnetostrictive materials, which can simultaneously operate as structural materials and actuators. The discovery of Delta-E effect in magnetostrictive materials has recently led to active vibration control via stiffness or resonance tuning. The Young's modulus level of magnetostrictive materials is much higher than that of other smart materials, for instance shape memory alloys and MR rubber [97]. Magnetically-variable springs have been developed and tested in the laboratory, but the effectiveness of these devices in practice is still under investigation. The nonlinearities of magnetostrictive materials, including hysteresis, anisotropy, and saturation, are one of the main challenges in magnetostrictive active vibration control, especially for multi-DOF vibration control systems (e.g., Stewart platforms). Advanced control algorithms are necessary to compensate for the material nonlinearities. Details of the control algorithms, which are not the scope of this article, can be found in the literature [98–100].

Passive dampers that consume no external power and require no controllers is another convenient option for vibration control. Magnetostrictive dampers can dissipate mechanical energy via magnetic hysteresis, magneto-mechanical coupling, and eddy currents. Compared with traditional passive damping materials, magnetostrictive materials is able to provide comparable loss factors while maintaining a high Young's modulus in GPa. As passive damping materials, magnetostrictive materials can be directly applied in the load path without increasing system compliance. Previous studies have investigated the damping effect due to the magnetic hysteresis loss alone. Terfenol-D exhibits a relatively large hysteresis but brittleness. To facilitate the bonding between fragile Terfenol-D and structural materials, flexible MPC have been developed. The hysteresis loss of Terfenol-D depends on material composition, crystal structure, and fabrication method. The FSZM fabrication and arc-melt fabrication are preferable for monolithic- and MPC-based dampers, respectively. Shunted magnetostrictive dampers that take advantage of all three energy dissipation mechanisms have recently been developed. A typical shunted magnetostrictive damper consists of a magnetostrictive element, coil, permanent magnet array, and electrical shunts. Even though Terfenol-D exhibits much higher magnetic hysteresis, Galfenol-based shunted dampers are able to provide larger loss factors due to its relatively higher saturation flux. The damping effect depends on finely-tuned bias conditions (e.g., pre-stress and permanent magnet strength) and the impedance of electrical shunts. The loss factor on the shunted magnetostrictive damper is maximized when the magnetostrictive element operates in the center of its burst region and an electrical resonance is created on a capacitive shunt circuit. In existing studies, the optimal capacitive load is selected manually and thus is sensitive to system uncertainties and environmental variations. Future studies should investigate resonance tracking techniques that can automatically ensure operation at electrical resonance. Eddy currents in the shunted magnetostrictive dampers induce additional Joule heating loss but also reduce magneto-mechanical coupling. Overall, eddy currents are detrimental to shunted magnetostrictive dampers and need to be avoided through lamination. However, eddy currents inside electrically-conductive magnetostrictive materials can facilitate compact and coil-less damper designs for tight locations and harsh environments where shunt circuits are infeasible. The mechanically-induced eddy currents and the resulting structural loss factor can be continuously tuned by adjusting the system bias conditions. Future studies should further investigate the possibility of implementing magnetostrictive materials as structural and tunable-damping materials at the same time.

Passive vibration control can be de-tuned when the system dynamics varies over time. Active vibration control is adaptive but requires complicate sensor arrangement, complex controller design, and large power sources. The unique material properties of magnetostrictive materials allow for semi-active control strategies where the drawbacks of passive and active control methods can be resolved. Most semi-active vibration control strategies based on magnetostrictive materials simply utilize the magnetostrictive actuator as a switch to trigger a larger control mechanism. Recent studies have discovered advanced semi-active control methods by using the aforementioned shunted magnetostrictive devices. Both the loss factor and the stiffness of the shunted magnetostrictive

device can be continuously adjusted via tuning the electrical impedance in the shunt circuit. Future studies can incorporate negative electrical shunt circuits with existing devices and further improve tunability. The tuning of shunt impedance can be self-sustainable, since part of the mechanical vibration energy can be scavenged from the shunt circuit.

Acknowledgments

ORCID iDs

Zhangxian Deng ⓘ https://orcid.org/0000-0003-1084-1738
Marcelo J Dapino ⓘ https://orcid.org/0000-0003-4888-1903

References

[1] Rao S S 2004 *Mechanical Vibrations* (Upper Saddle River: Prentice Hall)

[2] Inman D J 2017 *Vibration with Control* (New York: Wiley)

[3] Fuller C C, Elliott S and Nelson P A 1996 *Active Control of Vibration* (New York: Academic)

[4] Shahin A R, Meckl P H and Jones J D 1997 Modeling of SMA tendons for active control of structures *J. Intell. Mater. Syst. Struct.* **8** 51–70

[5] Giurgiutiu V 2000 Review of smart-materials actuation solutions for aeroelastic and vibration control *J. Intell. Mater. Syst. Struct.* **11** 525–44

[6] Bruant I, Gallimard L and Nikoukar S 2010 Optimal piezoelectric actuator and sensor location for active vibration control, using genetic algorithm *J. Sound Vib.* **329** 1615–35

[7] Song G, Sethi V and Li H-N 2006 Vibration control of civil structures using piezoceramic smart materials: a review *Engineering Structures* **28** 1513–24

[8] Hollkamp J J 1994 Multimodal passive vibration suppression with piezoelectric materials and resonant shunts *J. Intell. Mater. Syst. Struct.* **5** 49–57

[9] Vinogradov A M, Schmidt V H, Tuthill G F and Bohannan G W 2004 Damping and electromechanical energy losses in the piezoelectric polymer PVDF *Mech. Mater.* **36** 1007–16

[10] Ozbulut O E, Hurlebaus S and DesRoches R 2011 Seismic response control using shape memory alloys: a review *J. Intell. Mater. Syst. Struct.* **22** 1531–49

[11] Jalili N 2002 A comparative study and analysis of semi-active vibration-control systems *Journal of Vibration and Acoustics* **124** 593–605

[12] Giurgiutiu V, Chaudhry Z and Rogers C A 1995 Engineering feasibility of induced strain actuators for rotor blade active vibration control *J. Intell. Mater. Syst. Struct.* **6** 583–97

[13] Carlson J D and Jolly M R 2000 Mr fluid, foam and elastomer devices *Mechatronics* **10** 555–69

[14] Lai C Y and Liao W-H 2002 Vibration control of a suspension system via a magnetorheological fluid damper *Modal Analysis* **8** 527–47

[15] Asnani V M, Deng Z, Scheidler J J and Dapino M J 2016 Experimental comparison of piezoelectric and magnetostrictive shunt dampers *Proceedings of SPIE*

[16] Moffett M B, Clark A E, Wun-Fogle M, Linberg J, Teter J P and McLaughlin E A 1991 Characterization of Terfenol-D for magnetostrictive transducers *The Journal of the Acoustical Society of America* **89** 1448–55

[17] Clark A E, Wun-Fogle M, Restorff J B and Lograsso T A 2002 Magnetostrictive properties of Galfenol alloys under compressive stress *Materials Transactions* **43** 881–6

[18] Clark A, Hathaway K, Wun-Fogle M, Restorff J, Lograsso T A, Keppens V, Petculescu G and Taylor R 2003 Extraordinary magnetoelasticity and lattice softening in bcc Fe-Ga alloys *J. Appl. Phys.* **93** 8621–3

[19] Deng Z, Scheidler J J, Asnani V M and Dapino M J 2016 Quasi-static major and minor strain-stress loops in textured polycrystalline Fe81.6Ga18.4 Galfenol *J. Appl. Phys.* **120** 243901

[20] Goodfriend M and Shoop K 1992 Adaptive characteristics of the magnetostrictive alloy, Terfenol-D, for active vibration control *J. Intell. Mater. Syst. Struct.* **3** 245–54

[21] Dapino M J, Deng Z, Calkins F T and Flatau A B 2016 Magnetostrictive devices *Wiley Encyclopedia of Electrical and Electronics Engineering* (https://doi.org/10.1002/047134608X.W4549.pub2)

[22] Kellogg R, Flatau A B, Clark A, Wun-Fogle M and Lograsso T A 2002 Temperature and stress dependencies of the magnetic and magnetostrictive properties of Fe0.81Ga0.19 *J. Appl. Phys.* **91** 7821–3

[23] Wun-Fogle M, Restorff J and Clark A 2006 Magnetomechanical coupling in stress-annealed Fe-Ga (Galfenol) alloys *IEEE Trans. Magn.* **42** 3120–2

[24] Kornbluh R, Pelrine R, Pei Q, Oh S and Joseph J 2000 Ultrahigh strain response of field-actuated elastomeric polymers *Proc. SPIE (San Diego)* 3987 pp 0277–786X

[25] Moffett M B, Porzio R and Bernier G L 1995 High-power Terfenol-D flextensional transducer. Revision A *Tech. Rep.* DTIC Document

[26] Hartman S J 1997 Magnetostrictive system for high-frequency high-cycle fatigue testing *Tech. Rep.* University of Dayton Research Institute

[27] Deng Z 2017 Dynamic discrete energy-averaged model for magnetostrictive materials *J. Magn. Magn. Mater.* **441** 757–63

[28] Scheidler J J and Dapino M J 2016 Mechanically induced magnetic diffusion in cylindrical magnetoelastic materials *J. Magn. Magn. Mater.* **397** 233–9

[29] Restorff J, Wun-Fogle M and Summers E 2011 Hysteresis, d_{33}^* and d_{33} of Fe81Ga18.4 textured polycrystals *J. Appl. Phys.* **109** 07A922

[30] Evans P and Dapino M 2010 Efficient magnetic hysteresis model for field and stress application in magnetostrictive Galfenol *J. Appl. Phys.* **107** 063906

[31] Clark A E and Savage H 1974 Giant magnetically induced changes of the elastic moduli in tb0.3dy0.7fe2.0 *Technical Report* Naval Ordance Lab White Oak MD

[32] Savage H, Clark A and Powers J 1975 Magnetomechanical coupling and δE effect in highly magnetostrictive rare earth-Fe$_2$ compounds *IEEE Trans. Magn.* **11** 1355–7

[33] Kellogg R and Flatau A 2004 Wide band tunable mechanical resonator employing the δE effect of Terfenol-D *J. Intell. Mater. Syst. Struct.* **15** 355–68

[34] Kellogg R and Flatau A 2008 Experimental investigation of Terfenol-D's elastic modulus *J. Intell. Mater. Syst. Struct.* **19** 583–95

[35] Kellogg R A, Flatau A, Clark A E, Wun-Fogle M and Lograsso T 2003 Quasi-static transduction characterization of Galfenol *ASME 2003 International Mechanical*

Engineering Congress and Exposition (American Society of Mechanical Engineers) pp 273–80

[36] Atulasimha J, Flatau A B and Kellogg R A 2006 Sensing behavior of varied stoichiometry single crystal Fe-Ga *J. Intell. Mater. Syst. Struct.* **17** 97–105

[37] Wun-Fogle M, Restorff J and Clark A 2009 Soft and hard elastic moduli of Galfenol transduction elements *J. Appl. Phys.* **105** 07A923

[38] Datta S, Atulasimha J, Mudivarthi C and Flatau A 2010 Stress and magnetic field-dependent Young's modulus in single crystal iron-gallium alloys *J. Magn. Magn. Mater.* **322** 2135–44

[39] Scheidler J, Asnani V M, Deng Z and Dapino M J 2015 Dynamic characterization of Galfenol *Proceedings of SPIE*

[40] Scheidler J J, Asnani V M and Dapino M J 2016 Vibration control via stiffness switching of magnetostrictive transducers *Proceedings of SPIE*

[41] Snowdon J C 1968 *Vibration and Shock in Damped Mechanical Systems* (J. Wiley)

[42] Hiller M, Bryant M and Umegaki J 1989 Attenuation and transformation of vibration through active control of magnetostrictive Terfenol *J. Sound Vib.* **134** 507–19

[43] Mahapatra D R, Gopalakrishnan S and Balachandran B 2001 Active feedback control of multiple waves in helicopter gearbox support struts *Smart Mater. Struct.* **10** 1046

[44] Pelinescu I and Balachandran B 2001 Analytical study of active control of wave transmission through cylindrical struts *Smart Mater. Struct.* **10** 121

[45] Sutton T, Elliott S, Brennan M, Heron K and Jessop D 1997 Active isolation of multiple structural waves on a helicopter gearbox support strut *J. Sound Vib.* **205** 81–101

[46] Pratt J R, Oueini S S and Nayfeh A H 1997 Terfenol-D nonlinear vibration absorber *Proceedings of SPIE* pp 56–66

[47] Flatau A B, Hall D L and Schlesselman J M 1993 Magnetostrictive vibration control systems *J. Intell. Mater. Syst. Struct.* **4** 560–5

[48] Moon S-J, Lim C-W, Kim B-H and Park Y 2007 Structural vibration control using linear magnetostrictive actuators *J. Sound Vib.* **302** 875–91

[49] Rebbechi B, Howard C and Hansen C 1999 Active control of gearbox vibration *Proceedings of the Active Control of Sound and Vibration Conference (Fort Lauderdale)* pp 295–304

[50] Guan Y H, Li M, Lim T C and Shepard W S 2004 Comparative analysis of actuator concepts for active gear pair vibration control *J. Sound Vib.* **269** 273–94

[51] Bartlett P, Eaton S, Gore J, Metheringham W and Jenner A 2001 High-power, low frequency magnetostrictive actuation for anti-vibration applications *Sensors and Actuators A: Physical* **91** 133–6

[52] Yu Y, Naganathan N G and Dukkipati R V 2001 A literature review of automotive vehicle engine mounting systems *Mech. Mach. Theory* **36** 123–42

[53] Chakrabarti S and Dapino M J 2011 Hydraulically amplified Terfenol-D actuator for adaptive powertrain mounts *Journal of Vibration and Acoustics* **133** 061015

[54] Chakrabarti S and Dapino M J 2012 Coupled axisymmetric finite element model of a hydraulically amplified magnetostrictive actuator for active powertrain mounts *Finite Elem. Anal. Des.* **60** 25–34

[55] Chakrabarti S and Dapino M J 2010 A dynamic model for a displacement amplified magnetostrictive driver for active mounts *Smart Mater. Struct.* **19** 055009

[56] Nakamura Y, Nakayama M, Yasuda M and Fujita T 2006 Development of active six-degrees-of-freedom micro-vibration control system using hybrid actuators comprising air actuators and giant magnetostrictive actuators *Smart Mater. Struct.* **15** 1133

[57] Bryant M D, Fernandez B, Wang N, Murty V V, Vadlamani V and West T S 1993 Active vibration control in structures using magnetostrictive Terfenol with feedback and/or neural network controllers *J. Intell. Mater. Syst. Struct.* **4** 484–9

[58] Geng Z J and Haynes L S 1994 Six degree-of-freedom active vibration control using the stewart platforms *IEEE Trans. Control Syst. Technol.* **2** 45–53

[59] Nakamura Y, Nakayama M, Masuda K, Tanaka K, Yasuda M and Fujita T 1999 Development of active 6-DOF microvibration control system using giant magnetostrictive actuator *Proceedings of SPIE* pp 229–40

[60] Nakamura Y, Nakayama M, Kura M, Yasuda M and Fujita T 2007 Application of active micro-vibration control system using a giant magnetostrictive actuator *J. Intell. Mater. Syst. Struct.* **18** 1137–48

[61] Fujita T, Nonaka H, Yang C S, Kondo H, Mori Y and Amasaka Y 1998 Active vibration control of frame structures with a smart structure using magnetostrictive actuators *Proceedings of SPIE* pp 584–95

[62] Murty A K, Anjanappa M and Wu Y-F 1997 The use of magnetostrictive particle actuators for vibration attenuation of flexible beams *J. Sound Vib.* **206** 133–49

[63] Zhou H-M and Zhou Y-H 2007 Vibration suppression of laminated composite beams using actuators of giant magnetostrictive materials *Smart Mater. Struct.* **16** 198

[64] Shu L, Dapino M, Wu G and Chen D 2016 Frequency-dependent sliding-mode control of Galfenol-driven unimorph actuator based on finite-element model *IEEE Trans. Ind. Electron.* **63** 1071–82

[65] Scheidler J J and Dapino M J 2013 Nonlinear dynamic modeling and resonance tuning of Galfenol vibration absorbers *Smart Mater. Struct.* **22** 085015

[66] Bhattacharya B, Buravalla V R, Patsias S and Tomlinson G R 2000 Active and passive vibration control of flexible structures using a combination of magnetostrictive and ferromagnetic alloys *Proceedings of SPIE* pp 204–14

[67] Bandopadhya D, Bhattacharya B and Dutta A 2007 Modeling of hybrid damping scheme using smart magnetostrictive composites for flexible manipulator *J. Reinf. Plast. Compos.* **26** 861–80

[68] Chen M and Brennan M 2000 Active control of gear vibration using specially configured sensors and actuators *Smart Mater. Struct.* **9** 342

[69] Braghin F, Cinquemani S and Resta F 2012 A low frequency magnetostrictive inertial actuator for vibration control *Sensors and Actuators A: Physical* **180** 67–74

[70] May C, Kuhnen K, Pagliarulo P and Janocha H 2003 Magnetostrictive dynamic vibration absorber (DVA) for passive and active damping *Proceedings of the Euronoise (Citeseer)*

[71] Aurilio G, Cavallo A, Lecce L, Monaco E, Napolitano L and Natale C 2003 Fuselage frame vibration control using magnetostrictive hybrid dynamic vibration absorbers *Proceedings of Euronoise 2003 Conference (Napoli-ITALY)*

[72] Cavallo A, May C, Minardo A, Natale C, Pagliarulo P and Pirozzi S 2009 Active vibration control by a smart auxiliary mass damper equipped with a fiber bragg grating sensor *Sensors and Actuators A: Physical* **153** 180–6

[73] Scheidler J J, Asnani V M and Dapino M J 2016 Dynamically tuned magnetostrictive spring with electrically controlled stiffness *Smart Mater. Struct.* **25** 035007

[74] Deng Z, Asnani V M and Dapino M J 2015 Magnetostrictive vibration damper and energy harvester for rotating machinery *Proceedings of SPIE* pp 94330C–94330C

[75] Bozorth R M 1993 *Ferromagnetism, Ferromagnetism* (Wiley-VCH)

[76] Hathaway K, Clark A and Teter J 1995 Magnetomechanical damping in giant magnetostriction alloys *Metallurgical and Materials Transactions* A **26** 2797–801

[77] Teter J, Hathaway K and Clark A 1996 Zero field damping capacity in $(Tb_xDy_{1-x})Fe_y$ *J. Appl. Phys.* **79** 6213–5

[78] Wun-Fogle M, Restorff J B, Clark A E and Snodgrass J 2003 Magnetomechanical damping capacity of $Tb_xDy_{1-x}Fe_{1.92}(0.30 \leqslant x \leqslant 0.50)$ alloys *IEEE Trans. Magn.* **39** 3408–10

[79] Ho K K, Kerrigan C, Luna O and Carman G P 2005 Stoichiometric study of $Tb_xDy_{1-x}Fe_2$ particulate composites for passive damping *Proceedings of SPIE* pp 245–51

[80] Sandlund L, Fahlander M, Cedell T, Clark A, Restorff J and Wun-Fogle M 1994 Magnetostriction, elastic moduli, and coupling factors of composite Terfenol-D *J. Appl. Phys.* **75** 5656–8

[81] Pulliam W J, Lee D, Carman G P and McKnight G P 2003 Thin-layer magnetostrictive composite films for turbomachinery fan blade damping *Proceedings of SPIE* pp 360–71

[82] Scheidler J J, Asnani V M and Dapino M J 2016 Frequency-dependent, dynamic sensing properties of polycrystalline Galfenol (Fe81.6Ga18.4) *J. Appl. Phys.* **119** 244902

[83] Deng Z, Zhang Q and Dapino M 2018 Dynamic model for magnetostrictive systems with applications to damper design *IEEE/ASME Trans. Mechatronics* **23** 1823–31

[84] Deng Z, Asnani V, Scheidler J and Dapino M 2018 Shunted magnetostrictive devices in vibration control *IEEE/ASME Trans. Mechatronics* in preparation

[85] Davino D, Giustiniani A, Visone C and Adly A 2011 Experimental analysis of vibrations damping due to magnetostrictive based energy harvesting *J. Appl. Phys.* **109** 07E509

[86] Fenn R C and Gerver M J 1994 Passive damping and velocity sensing using magnetostrictive transduction *Proceedings of SPIE* pp 216–27

[87] Kerrigan C, Ho K, Mohanchandra K and Carman G 2008 Sputter deposition and analysis of thin film Nitinol/Terfenol-D multilaminate for vibration damping, Smart *Materials and Structures* **18** 015007

[88] Ohmata K, Zaike M and Koh T 1997 A three-link arm type vibration control device using magnetostrictive actuators *J. Alloys Compd.* **258** 74–8

[89] Fenn R, Downer J, Dushko D, Gondhalekar V and Ham N 1996 Terfenol-D driven flaps for helicopter vibration reduction *Smart Mater. Struct.* **5** 49

[90] Flatau A B, Dapino M J and Calkins F T 2000 High bandwidth tunability in a smart vibration absorber *J. Intell. Mater. Syst. Struct.* **11** 923–9

[91] Braghin F, Cinquemani S and Resta F 2011 A model of magnetostrictive actuators for active vibration control *Sensors and Actuators A: Physical* **165** 342–50

[92] Scheidler J J and Asnani V M 2017 Validated linear dynamic model of electrically-shunted magnetostrictive transducers with application to structural vibration control *Smart Mater. Struct.* **26** 035057

[93] Deng Z 2015 Nonlinear modeling and characterization of the Villari effect and model-guided development of magnetostrictive energy harvesters and dampers *Ph.D. Dissertation* The Ohio State University

[94] Yoo J, Murray A and Flatau A B 2014 Evaluation of magnetostrictive shunt damper performance using iron (Fe)-gallium (Ga) alloy *Proceedings of SPIE* pp 90573I–90573I

[95] Deng Z and Dapino M J 2017 Review of magnetostrictive vibration energy harvesters *Smart Mater. Struct.* **26** 103001

[96] Deng Z and Dapino M J 2017 Magnetic flux biasing of magnetostrictive sensors *Smart Mater. Struct.* **26** 055027

[97] Harne R L, Deng Z and Dapino M J 2017 Adaptive magnetoelastic metamaterials: A new class of magnetorheological elastomers *J. Intell. Mater. Syst. Struct.* **29** 265–78

[98] Zhang T, Jiang C, Zhang H and Xu H 2004 Giant magnetostrictive actuators for active vibration control *Smart Mater. Struct.* **13** 473

[99] Shaw J 1998 Adaptive vibration control by using magnetostrictive actuator *J. Intell. Mater. Syst. Struct.* **9** 87–94

[100] Oates W S and Smith R C 2008 Nonlinear optimal control techniques for vibration attenuation using magnetostrictive actuators *J. Intell. Mater. Syst. Struct.* **19** 193–209